Fabrication of $CuInSe_2$ Thin Film Solar Cells

Byung Tae Ahn and Jinsoo Song*

Department of Materials Science and Engineering, KAIST, Taejon, Korea

*New Energy Department, Korea Institute of Energy Research, Taejon, Korea

ABSTRACTS

This paper presented the trend of CIS solar cell development and the current status of CIS cell research conducted by the collaboration of KAIST and KIER.

I. Introduction

The commercial solar cells available at the present days are fabricated using the materials such as single crystal Si wafer, polycrystalline Si wafer, amorphous Si film, and CdTe film. In 1998, the world solar cell productions by the materials were 60, 67, 19, and 7 MW, respectively. In 1999, the total production was 201.5 MW. More than 80% of total world production was covered by the Si solar cells: both single crystal and polycrystalline cells. The world market in 1999 was 2b$ and is expected to be 24b$ in 2010[1,2].

The module price of Si solar cells has been continuously reduced along with the increase of the module efficiency of Si solar cells (Fig.1)[3]. However, the module price is nearly saturated to about 4$/Wp after the year 1990, which should be lowered below 1$/Wp to compete with commercial electric power. The costs of Si ingot and wafering cover between 55% and 65% of that of Si solar cells. To avoid the limit of Si material cost, it is necessary to develop thin-film solar cells such as amorphous Si, CdTe, and

$CuInSe_2$. The expected module price of these thin film cells is ranging from $1.20 to $2.00/Wp after the year 2000. The price is expected to be about $1/Wp after 2010.

Amorphous Si cell has been the most popular cell among thin-film solar cells for last two decades as the replacement of Si cells. However, the degradation of cell efficiency was the major problem and remained to be solved. Also one of the hottest thin-fim solar cells for the last 10 years has been $CuInSe_2$–based cells whose solar efficiency was drastically improved (Fig. 2)[4,5]. The efficiency from 10% to 20% for the last 10years. The efficiency of 20% can be considered as very high since the highest efficiency of single crystal Si cell is 25%[6]. Unlike a-Si , no degradation of cell efficiency has been observed in the CIS cells. NREL, EUROCIS, and Matsushita are leading groups in high-efficiency CIS research and Siemens Solar, EPV, Showa Shell, IPE/ZSW, and Matsushita are producing prototype modules with efficiency of about 13%, which is close to the module efficiency of commercially available Si solar cells (14%)[7,8]. It is expected that the production of thin film solar cells such as CIS, CdTe, and stacked poly-Si will dominate Si solar cells in the year 2010.

In Korea, KAIST conducted the research on CIS cells for last 10 years. But reasonable efficiencies have been achieved only within last three years by collaborating with KIER. This paper reviewed CIS solar cell research conducted by the collaboration of KAIST and KIER.

2. Fabrication of CIS Cells

Fig. 3 shows the structure of CIS solar cell. It consists of Al/n-ZnO/i-ZnO/CdS/ $Cu(In_{1-x}Ga_x)Se_2$/Mo/glass substrate. A 1μm-thick Mo film was prepared by DC magnetron sputtering for back contact. The resistivity of the film deposited at 2 mTorr

was $5x10^{-5}$ Ω·cm. The CIS layer was deposited by three-stage co-evaporation method[9]. The CdS buffer layer (80nm) was prepared by chemical bath deposition. i-ZnO(50nm) and n-ZnO(1μm) films were prepared by RF magnetron sputtering for use as a window layer. The resistivity and the transmittance of i- and n-ZnO film were $5x10^{-4}$ Ω·cm and above 85%, respectively.

In the structure, the most critical layer is the light absorbing CIGS layer. Ga is added to increase the bandgap of CIS materials. The layer was prepared with a process named as three-stage process. Fig. 4 shows the temperature profile of the process. Firstly, In, Ga, and Se elements are co-evaporated on Mo-coated glass substrates at 350°C. $(In_{1-x}Ga_x)Se_y$ layer is deposited at this stage. Secondly, Cu and Se elements are co-evaporated at 550°C. The Cu and Se source directly react to form $Cu((In_{1-x}Ga_x)Se_2$ compound at this stage. The morphology can be improved by controlling the stoichiometry of CIS as Cu-rich. Thirdly, In, Ga, and Se elements are co-evaporated at 550°C to produce an In-rich layer on the CIS film. Note that the CIS film consists of Cu-rich bottom layer and In-rich top layer. The overall CIS composition was controlled by adjusting the deposition time at each stage. All the films were deposited in a vacuum of about 10^{-7} Torr.

3. CIS cells

Fig. 5 shows the cross-sectional SEM morphologies of 2μm-thick CIS films on Corning glass with the average Cu/In ratio of 1.18(a), 0.98(b), and 0.83(c). The CIS films with large Cu/In ratios have large grains and large grooves between the grains. As the Cu/In ratio decreases, the grain size at surface becomes smaller and the layer with small grains becomes thicker[10].

Fig. 6 shows the AES depth profile of the CIS film with a Cu/In ratio of 0.98. The layer with small grains near the film surface is In-rich, while the layer with large grains on the bottom is Cu-rich. The composition ratio at the surface indicates that $CuIn_3Se_5$ phase is formed. The formation of bi-layer is very important to achieve a pn junction characteristics[11].

Fig. 7 shows the J-V curves of the solar cell using CIS films with the ratio of 0.95 with the structure of Al/ITO/ZnO/In_2Se_3/CIS/Mo. The resulting solar efficiency of 8.12% was obtained with the cell parameters (Voc = 399mV, Jsc = 38.25mA/cm^2, and FF = 0.53) when thin $CuIn_3Se_5$ layer was formed on the top of the $CuInSe_2$ film. With no Ga addition, the efficiency of 8.12% is generally considered as very high efficiency. The cell performance was limited by the poor interface properties at the In_2Se_3/ZnO interface with possible high recombination sites, resulting in the low open circuit voltage and fill factor.

4. CIGS solar cells

To increase to Voc, it is necessary to increase the bandgap energy of CIS layer by the addition of Ga. Fig. 8 shows the optical transmittance of CIGS films as a function of Ga/(In+Ga) ratio. As the ratio increases the bandgap of CIGS film increases from 1.04 to 1.64 eV and the absolute transmittance decreases. The reduction of transmittance is due to smaller grain size as the Ga content increases.

Fig. 9 shows the electrical resistivity of the CIGS films as a function of Cu/$In_{0.5}Ga_{0.5}$ ratio on Corning glass and soda-lime glass substrates. The CIGS films on Corning glass exhibit a wide range of resistivity from 10 to 10^5 Ω·cm. But the CIGS films on soda-lime glass show the resistivity of about 10 Ω·cm when the Cu/$In_{0.5}Ga_{0.5}$ ratio is less

than 0.95 and that of about 1 Ω·cm when the $Cu/In_{0.5}Ga_{0.5}$ is larger than 1.0. Note that in the Cu-deficient compositions the resistivity of CIGS films on soda-lime glass is much lower than that of CIGS films on Corning glass. The Hall measurement indicated that the reason of low resistivity was due to the increase of carrier concentration[12].

Fig. 10 shows the SIMS Na depth profiles of CIGS films prepared on the Mo-coated soda-lime glass substrate as a function of $Cu/In_{0.5}Ga_{0.5}$ ratio. All CIGS films show the incorporation of Na in the bulk layer and the accumulation of Na at the surface. The overall concentration of Na in the bulk layer is relatively uniform and the value does not change significantly with various Cu/(In+Ga) ratios. The Na incorporation in the bulk CIGS layer greatly stabilizes the carrier concentration in the range of $10^{16}/cm^3$, which is an optimum carrier concentration for optical absorbing layer.

The surface accumulation of Na causes the depletion of Cu at the surface due to exchange between Cu and Na. The surface accumulation of Na may be related to the reactivity of Na with oxygen. The XPS depth profile of Se and Na of the CIGS films indicated that Na at the surface was oxidized and Na_2SeO_3 was formed[4,5]. This indicates that Na in the bulk of CIGS films diffuses toward surface as soon as samples are exposed to air, resulting in the reaction of Na with oxygen.

Fig. 11 shows the J-V curves of Ag/n-ZnO/i-ZnO/CdS/CIGS/Mo/glass solar cells with active areas of 0.18 and 0.88 cm^2. In the case of large active area, the series resistance of devices increased, and the shunt resistance decreased. As a result, increasing the active area reduces efficiency of solar cells. The effect of area is an important factor to determine the area of solar cells modules. The currently best efficiency in this study is 14.48% for 0.18 cm^2 (Voc = 581.5 mV, Jsc = 34.88 mA, F.F = 0.714).

5. Future works

It is necessary to analyze the efficiency loss factors to further improve the solar efficiency. To enhance the evaporation rate of Cu, In, and Ga, binary selenide compounds such as Cu_2Se, In_2Se_3, and Ga_2Se_3 can be utilized. At the present time the basic understanding and efficiency improvement of CIS cell have been mainly focused. For low-cost large-area commercial cells, the CIGS layer should be fabricated by sputtering method.

References

1. Photovoltaic News, Vol. 19, No. 2, Feb., (2000).
2. E.C : Photovoltaics in 2010, European Photovoltaic Industry Association (1996).
3. IT Power : Electricity from Sunlight, UK, (1997).
4. M. Konagai, Technical Digest of Intern. PVSEC-11, Hokkaido, Japan (1999) 25.
5. J. E. Rannels, Technical Digest of Intern. PVSEC-11, Hokkaido, Japan (1999) 9.
6. M. A. Green, J. Zhao, A. Wang, and S. R. Wenham, Technical Digest of Intern. PVSEC-11, Hokkaido, Japan (1999) 21.
7. P. Maycock : Renewable Energy World, Vol. 2, No. 4, July, (1999).
8. K. Masuda, Technical Digest of Intern. PVSEC-11, Hokkaido, Japan (1999) 5.
9. M. A. Contreras, A. M. Gabor, A. L. Tennant, A. Asher, J. R. Tuttle, R. Noufi, Prog. Photovoltaics 2, (1994) 287.
10. S. H. Kwon et al., J. Korean Phys. Soc. Vol. 31, No. 5 (1997) 796.
11. S. H. Kwon et al. Thin Solid Films, Vol. 323 (1998) 265.
12. S. H. Kwon et al. Technical Digest of Intern. PVSEC-11, Hokkaido, Japan (1999) 71.

Figure captions

Fig. 1. Trend of module price and module efficiency of Si solar cells.

Fig. 2. Trend of CIS cell efficiency.

Fig. 3. Structure of CIS cells.

Fig. 4. Temperature profile of three-stage coevaporation process for CIS film formation.

Fig. 5. Cross-sectional SEM morphologies of CIS layer with various Cu/In ratios: (a) 1.18, (b) 0.98, and (c) 0.83.

Fig. 6. AES depth profiles of CIS film with Cu/In = 0.98.

Fig. 7. J-V curves of In_2Se_3/CIS cell.

Fig. 8. Optical transmittance of CIGS films with various Ga/(In+Ga) ratios.

Fig. 9. Electrical resistivity with various Cu/(In+Ga) ratios.

Fig. 10. SIMS depth profile of Na in CIGS films prepared on Mo/soda-lime glass substrate.

Fig. 11. J-V curves of CdS/CIGS cells.

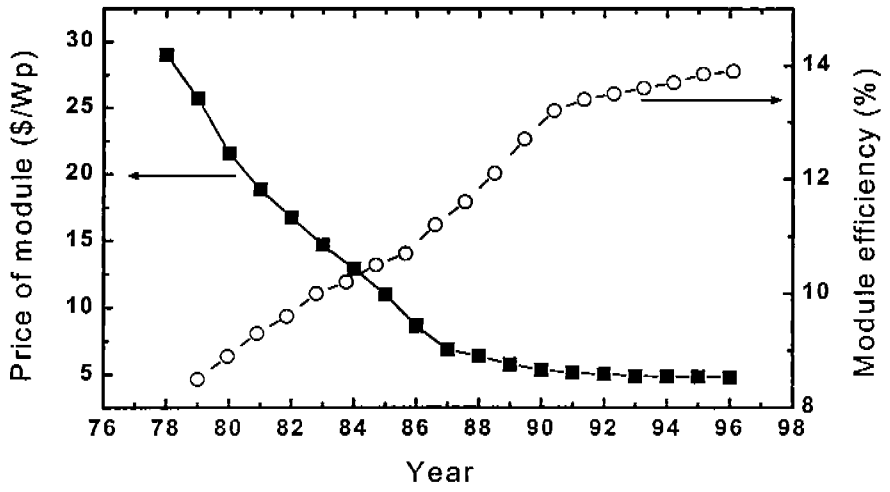

Fig. 1. Trend of module price and module efficiency of Si solar cells.

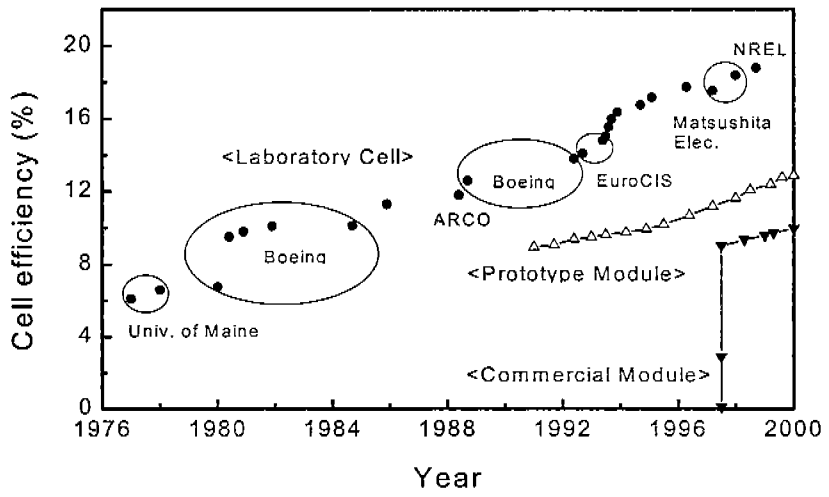

Fig. 2. Trend of CIS cell efficiency.

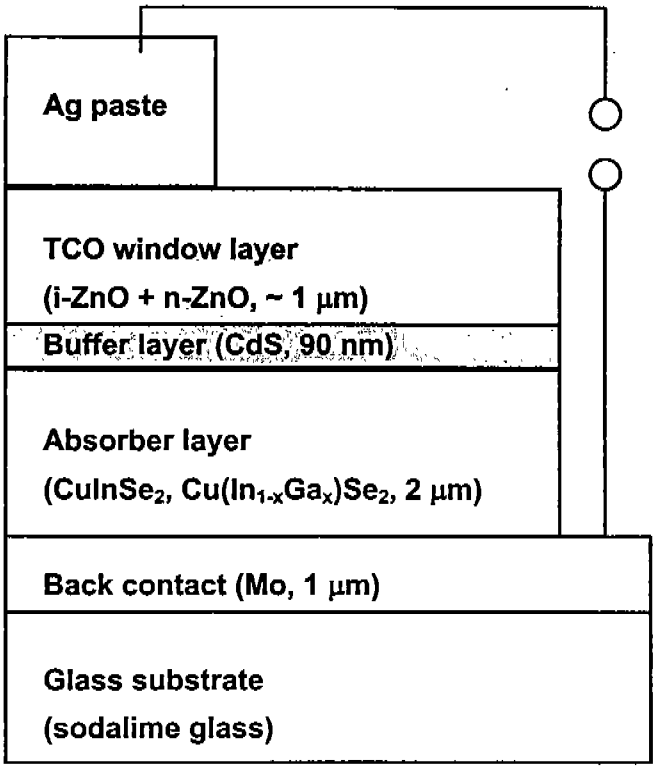

Fig. 3. Structure of CIS cells.

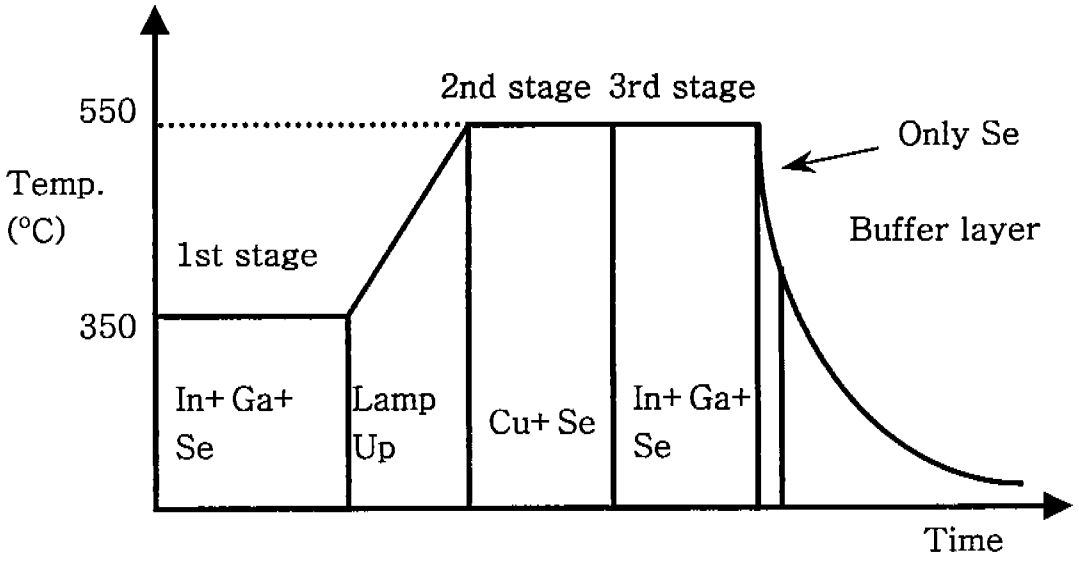

Fig. 4. Temperature profile of three-stage coevaporation process for CIS film formation.

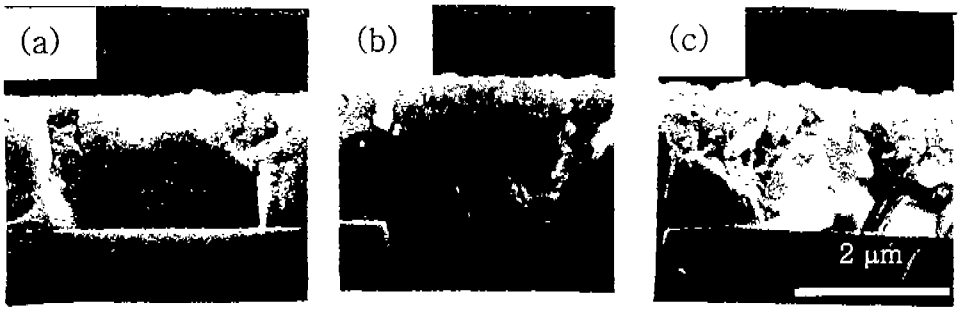

Fig. 5. Cross-sectional SEM morphologies of CIS layer with various Cu/In ratios : (a) 1.18, (b) 0.98, and (c) 0.83.

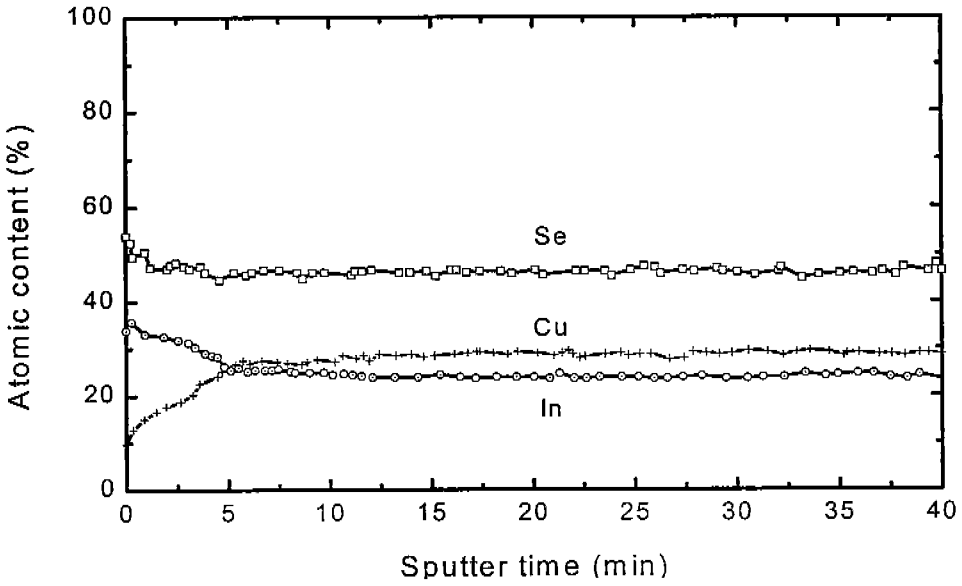

Fig. 6. AES depth profiles of CIS film with Cu/In = 0.98.

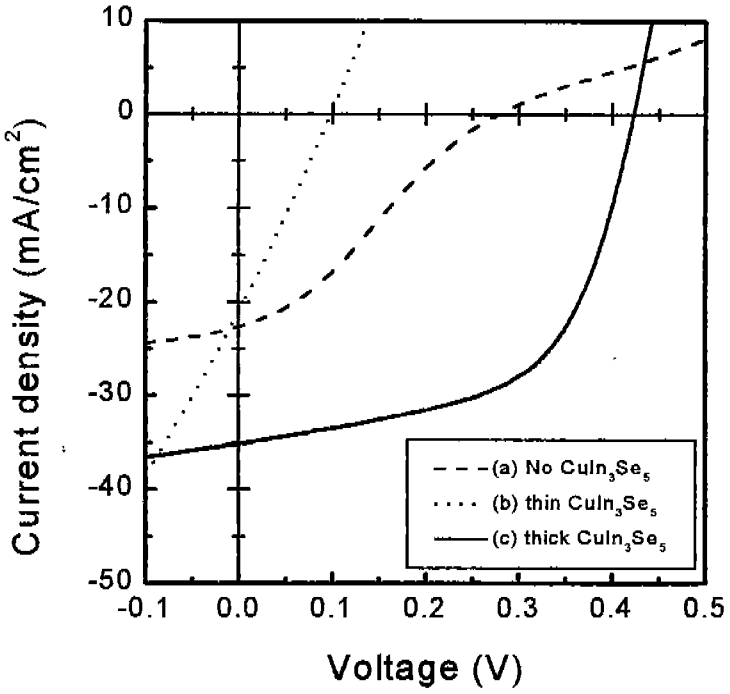

Fig. 7. J-V curves of In_2Se_3/CIS cell.

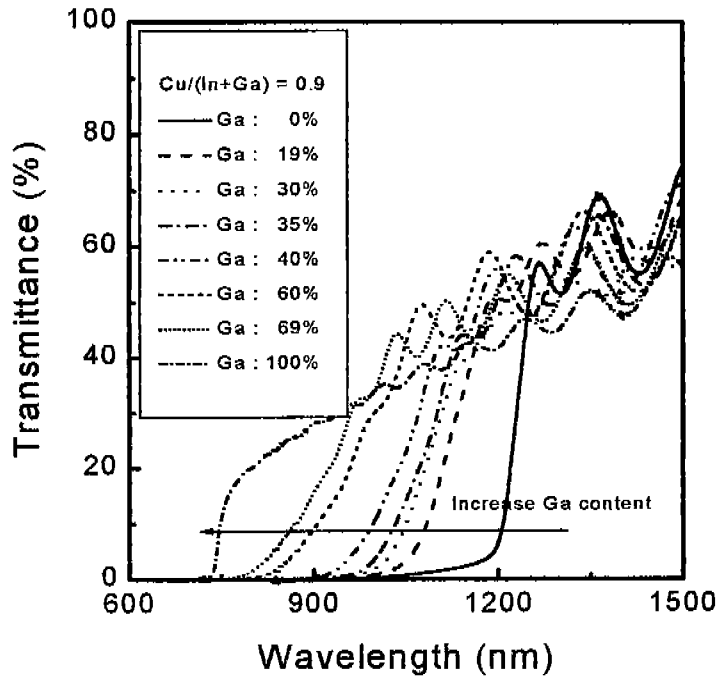

Fig. 8. Optical transmittance of CIGS films with various Ga/(In+Ga) ratios.

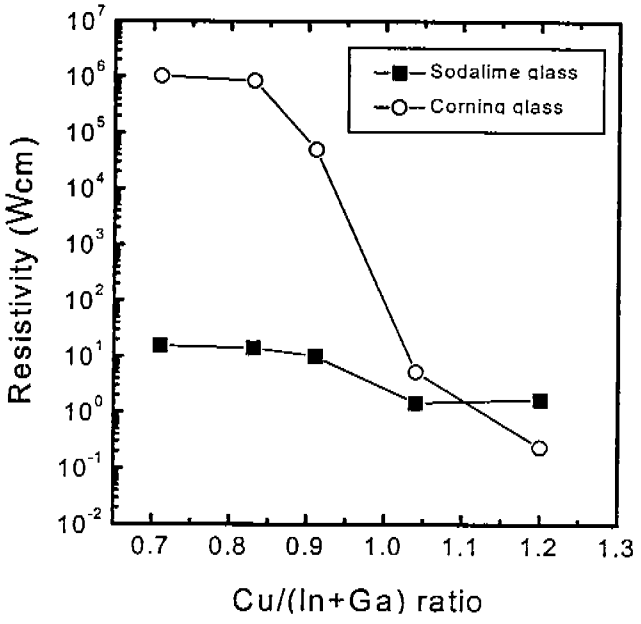

Fig. 9. Electrical resistivity with various Cu/(In+Ga) ratios.

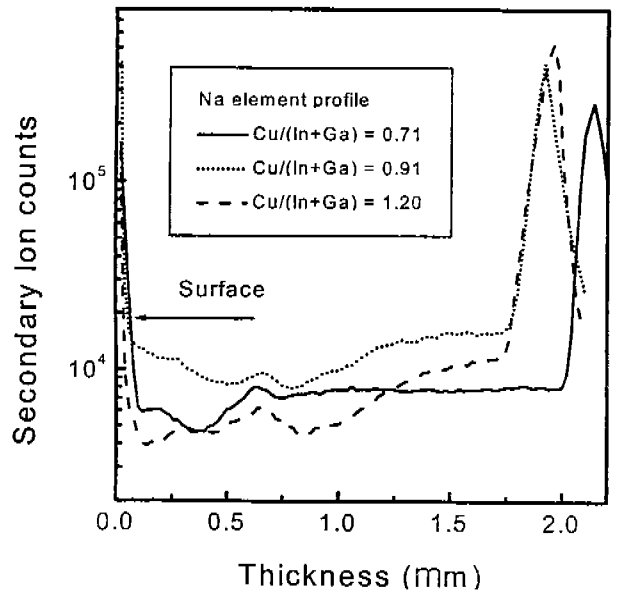

Fig. 10. SIMS depth profile of Na in CIGS films prepared on Mo/soda-lime glass substrate

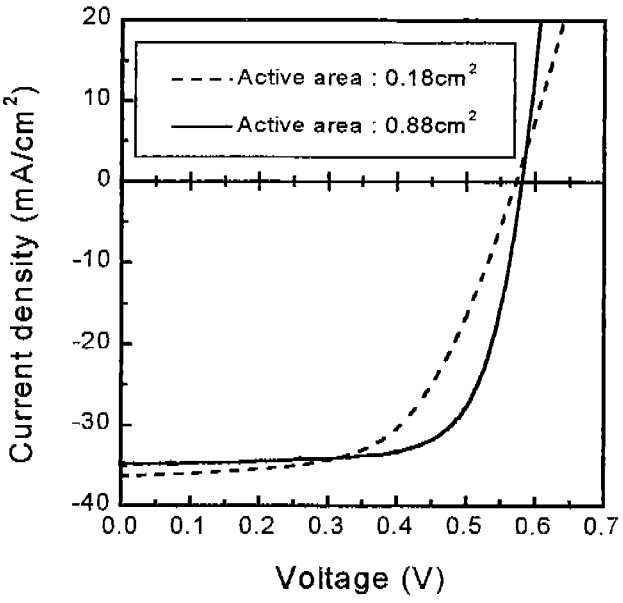

Fig. 11. J-V curves of CdS/CIGS cells.